Journal of Biomaterials Science, Polymer Edition

ISSN: 0920-5063 (Print) 1568-5624 (Online) Journal homepage: https://www.tandfonline.com/loi/tbsp20

Mechanical strong stretchable conductive multi-stimuli- responsive nanocomposite double network hydrogel as biosensor and actuator

Yang Chen, Wenwen Wu, Junrong Yu, Yan Wang, Jing Zhu & Zuming Hu

To cite this article: Yang Chen, Wenwen Wu, Junrong Yu, Yan Wang, Jing Zhu & Zuming Hu (2020): Mechanical strong stretchable conductive multi-stimuli- responsive nanocomposite double network hydrogel as biosensor and actuator, Journal of Biomaterials Science, Polymer Edition, DOI: 10.1080/09205063.2020.1775760

To link to this article: https://doi.org/10.1080/09205063.2020.1775760

Accepted author version posted online: 28 May 2020.

Mechanical strong stretchable conductive multi-stimuli- responsive nanocomposite double network hydrogel as biosensor and actuator

Yang Chen, Wenwen Wu, Junrong Yu*, Yan Wang, Jing Zhu and Zuming Hu

State Key Laboratory for Modification of Chemical Fibers and Polymer Materials, College of Materials Science and Engineering, Donghua University, Shanghai 201620, China

*Correspondence to: Junrong Yu (E-mail: yjr@dhu.edu.cn)

Abstract

Multi-stimuli- responsive mechanical strong stretchable hydrogel has grabbed extensive attention in recent years. Here, a novel stretchable conductive biocompatible near-infrared light(NIR)-/thermal-/pH-/ionic concentration- responsive carboxymethyl chitosan (CMCTs)/graphene oxide (GO)/poly(N-isopropylacrylamide)(PNIPAm) nanocomposite double network hydrogel was fabricated through a simple one-pot in situ free radical polymerization, which is initiated by ultraviolet (UV) light and using N-(3-dimethylaminopropyl)-N-ethylcarbodiimidehydrochloride (EDC) and N,N'-bis(acryloyl)cystamine (BAC) as cross-linkers respectively, instead of toxic organic molecules. When the concentration of CMCTs, GO, EDC and BAC is 22.50, 0.103, 7.50 and 0.467 mg/mL respectively, the obtained hydrogel sample owns the highest tensile strength of 1046 kPa at failure strain of 1286 % and a corresponding compressive stress of 2.37 MPa at deformation of 90 %. Besides, these hydrogels have an obvious pH-/thermal-/ionic concentration- responsive properties depending on the concentration of the above mentioned factors, and their good conductive property makes them as candidate material for healthcare biosensors. Finally, we attempt to design a novel thermal-/NIR-responsive double network structure bilayer hydrogel, which has the potential use as remote actuator

in dangerous places in the future.

Key words: multi-stimuli- responsive, carboxymethyl chitosan, mechanical strong, hydrogel, ionic conductivity

1 Introduction

Smart hydrogels, prominently changing their volume, transparence, color or other properties with reference to external stimuli such as temperature[1] , pH[2,3], light[4,5], electric field[6,7], magnetic field[8,9], humidity[10] and ionic[11] etc, have captured considerable attention in recent years. Due to these above excellent properties, smart hydrogels have exhibited pronounced potential in large amounts of applications, such as biosensors[12], actuators[13], drug delivery carriers[14], as well as artificial muscles[15,16] and tissue engineering scaffolds[17]. But, these hydrogels usually suffer from two defects: weak mechanical property and single stimuli-responsiveness, which greatly restrict their applications, how to synthesize the mechanical strong multi-stimuli- responsive hydrogel has attracted a great deal of interest in recent scientific research reports.

For the former, plenty of strategy has been adopted to design mechanical strong stretchable hydrogels in the last decade, such as hydrophobically associated hydrogels[18], supermolecular hydrogels[19], nanocomposite (NC) hydrogels[20], double cross-linked (DC) hydrogels[21] and double network (DN) hydrogels[22]. Among the above listed hydrogels, NC, DC and DN hydrogels have been more often used to synthesize mechanical strong hydrogels. Gao et al.[23] have synthesized the self-healable, tough and ultra-stretchable polyacrylamide (PAM)/montmorillonite (MMT) NC hydrogel, using MMT nanosheets as

crosslink centers, which owns the highest tensile strength about 175 kPa and the corresponding breaking elongation of 11800%. Shi et al.[24] have prepared the near-infrared light-responsive PNIPAm/GO NC DC hydrogel with the highest tensile strength about 750 kPa at failure strain of 2500 %. Chen et al.[12] have fabricated the PAM/silk fibroin fully physical network structure DN hydrogels, which have the highest breaking tensile strength about 1.17 MPa. Owing to these good conductive and stretchable properties, they could be used as strain biosensors.

For the latter, manufacturing the semi-interpenetration network (semi-IPN) or interpenetration network (IPN) is an effective way to integrate the properties of two different materials. Huang et al.[25] have synthesized the semi-IPN PNIPAm/chitosan/GO NC hydrogel with good pH- and temperature- responsive property. With the addition of GO nanosheets, its mechanical properties have been improved obviously. Chen et al.[26] have fabricated the semi-IPN poly(dimethylaminoethyl methacrylate)/CMCTs hydrogel using clay nanosheets as cross-linkers, which can be used as drug deliver carrier of theophylline. Chen et al.[27] have prepared the mechanical strong pH-/temperature- responsive CMCTs/PNIPAm nanocomposite double network (a special case of IPN network) hydrogel, using genipin and clay as the cross-linkers to crosslink CMCTs and PNIPAm polymer chains respectively, which has the highest breaking tensile strength about 137 kPa at the failure strain of 446.1 %.

CMCTs, an important derivant of chitosan, is an amphoteric polyelectrolyte material, owning obvious pH-responsive and good ionic conductivity property in theory. Under acidic condition, EDC and NHS were often used as bio-cross-linkers to link carboxyl and amino groups on the CMCTs polymer chains to synthesize hydrogels, however, most of these

obtained hydrogels are brittle and mechanical weakness, which greatly restricts their applications[28,29]. N-isopropylacrylamide is frequently used as thermo-sensitive monomer to fabricate temperature-responsive hydrogels. When it was mixed with photo-thermal conversion nanoparticles, such as graphene oxide[30], gold[31], polydopamine[20] and carbon nanotubes[32] etc, these synthesized hydrogels often possess good NIR- responsive property and could be used as remote NIR controllers.

According to the above description, we attempt to fabricate a novel biocompatible mechanical strong conductive stretchable NIR-/thermal-/pH-/ionic concentration- responsive CMCTs/GO/PNIPAm NC DN hydrogel through a simple one-pot *in situ* free radical polymerization triggered by UV light, using biological molecules (EDC and BAC) to crosslink CMCTs/GO and PNIPAm polymer chains, respectively. The optimal robust tough stretchable hydrogel could be obtained by manipulating the following critical factors: the concentration of BAC, EDC, CMCTs and GO. Furthermore, the optimum hydrogel is stretchable and conductive, and its resistance varies gradually with the strain under recycle tensile or compressive tests. This property makes it to be used as healthcare strain biosensors in future. In addition, we try to design novel double network structure bilayer hydrogel sample, in which the two layers own different crosslink density by adjusting the concentration of the above mentioned crucial factors. These bilayer hydrogel samples not only have evidently thermal-responsive property but pronounced NIR responsive bending property, which may have potential use in actuator, such as remote controller in dangerous place in future.

2 Characterization and synthesis

2.1 Materials and characterization

2.1.1 Materials

CMCTs(with the substitution degree of 0.92 and viscosity-average molecular weight of 361 kDa) and GO were synthesized as referred in our previous work[33]. NIPAm (J&K Scientific Co., Ltd., China) was recrystallized from a toluene/n-hexane mixture solution and dried in vacuum at 40℃ before used. BAC was bought from Alfa Aesar Co., Ltd. 2-hydroxy-4'-(2-hydroxyethoxy)-2-methylpropiophenone (I2959) was supplied by the Tokyo Chemical Industry Co., Ltd., Japan. EDC, NHS and 4-morpholineethanesulfonic acid (MES) were supplied by Sigma-Aldrich Co., Ltd., America. Sodium hydroxide (NaOH), sodium dihydrogen phosphate (NaH_2PO_4), disodium hydrogen phosphate (Na_2HPO_4), and phosphoric acid were all obtained from Sinopharm Chemical Reagent Co., Ltd., China.

2.1.2 Characterization

The UV-vis spectra were carried out by the spectrophotometer (Thermo SCIENTIFIC, Biomate 3S, USA) instrument from 190 to 400 nm. Raman spectra were measured by an Invia-Reflex spectrometer (U.S.A) with 532 nm laser excitation. X-ray diffraction (XRD) tests were conducted on a XRD instrument (Japan) using Cu kα radiation (λ = 0.154 nm) in a step of $0.02°s^{-1}$, ranging from 5°to 60°.

After immersed into the deionized water for two weeks (changing water three times a day), and freeze drying, the internal cross-section morphology of CGPH was examined on Quanta 250 (FEI Company, U.S.A) environment scanning electron microscope (ESEM) at the voltage

of 10 kV.

The conductivity of hydrogel samples was recorded by electrochemical workstation at the voltage of 1 V.

2.2 Sythesis of hydrogel and bilayer hydrogel actuator

2.2.1 Synthesis of CMCTs/GO/PNIPAm NC DN hydrogels

The synthesis process of CMCTs/GO/PNIPAm NC DN hydrogel is schematically shown in Fig. 1 and its corresponding image was displayed in Fig. S1. At first, a given amount of GO aqueous (5.15 mg/mL) was gradually added into a calculated amount of MES (0.64M) aqueous solution under the stirred condition. Followed by, a predetermined weight of CMCTs was added in and the mixed solution was continued stirred for 22 h at room temperature. Secondly, 0.59 g NIPAm, 5.60 mg initiator (I2959) and a certain weight of BAC were added in and the mixture solution was stirred for another 1.5h. Subsequently, a quantitative amount of EDC/NHS (with the molar ratio of 4:1) was added in and the obtained solution was stirred in ice-water bath for the last 30 min to get a uniform solution. At last, the above solution was pumped and refilled with nitrogen 3 times, and then was transferred into the designed transparent mold. Successively, the sealed mold was put into 20℃water bath and the mixture solution was reacted for 20 h to get the EDC cross-linked CMCTs/GO network. Afterwards, the above mold was irradiated by UV light (365 nm) with the power of 6 W for 2 h to achieve the mechanical strong stretchable CMCTs/GO/PNIPAm NC DN hydrogels, rotating the mold 180°per 30 min.

The above synthesized NC DN hydroels are denoted as $C_mG_nP_{x-y}H$, where C, G, P and H

represents for CMCTs, GO, PNIPAm and hydrogels respectively, and m, n, x and y stands for the concentration of CMCTs, GO, EDC and BAC respectively. For example, $C_{25}G_{0.103}P_{10\text{-}0.266}H$ means that in this fabricated hydrogel sample, the concentration of CMCTs, GO, EDC and BAC is 25 mg/mL, 0.103 mg/mL, 10 mg/ml and 0.267 mg/mL (All formulations of reagents for the synthesis of the representative hydrogel samples are listed in Table 1). Among all the prepared hydrogel samples, the total water content is fixed at 5 mL.

2.2.2 Synthesis of the bilayer hydrogel actuator

As illustrated in Fig.1, when the first layer's mixture was transferred into the rectangular mold, it was flattened by a slide and reacted for a few minutes under the catalysis of EDC/NHS. Before fully completed cross-linked, the second layers' mixture (with different component) was added into the second same thickness rectangular mold (which is put on the first mold), and flattened with another slide. After reacted at the room temperature for 24 hours, the bilayer hydrogel actuator was achieved by irradiated under the UV light for 2 h.

2.2.3 Crucial factors for preparing homogeneous mechanical strong hydrogels

During the hydrogel preparation process, we take 365 nm UV light as the initiated light resource. In order to verify whether GO and BAC aqueous solutions has strong absorption of 365 nm ultraviolet light, ultraviolet-visible spectra of different concentrations GO and BAC aqueous solutions were scanned (as shown in Fig. S2). It can be clearly seen that BAC aqueous solution has very weak absorption of 365 nm UV light (its absorption intensity is near to zero), and the absorption intensity increases only a little as its concentration increase greatly. These results demonstrate that 365 nm UV light may have little damage to the

disulfide bonds in BAC molecules and the effective cross-linked PNIPAm flexible polymer chains could be formed in synthesized hydrogels. The latter mechanical tested hydrogel samples (in section 3.3) having large recoverable strain and high mechanical strength indicates that most of the disulfide bonds are preserved and they are benefit to form the effective cross-linked flexible PNIPAm polymer networks in the synthesized hydrogels. Furthermore, GO aqueous solution has strong absorption of 365nm UV light and the absorption intensity increase greatly as its concentration increases, which defines that GO content in the synthesized hydrogel should not be too high or its strong absorption of UV light make incomplete decomposition of I 2959, resulting in uneven cross-linked PNIPAm polymer chains, and lower crosslink density and mechanical strength. In conclusion, to some extent, a certain content of GO nanosheets may play a role in protecting disulfide bonds in BAC molecule and ensure the formation of flexible and effective cross-linked PNIPAm polymer networks.

Because CMCTs are prepared under alkaline conditions, large amounts of -COONa are existed on CMCTs polymer chains. In order to ensure the smooth progress of reaction, CMCTs must be immersed in acid solution for enough time to make -COONa successfully converse to -COOH[34]. Besides, the surface formed PNIPAm polymer of hydrogel sample is easy to shrink and become opaque after heat absorption (UV light supplied), which results in reaction of NIPAm inside the sample couldn't be continued (no UV light, no I2959 decomposed). So that these obtained hydrogel samples are usually uneven (as shown in Figure S3a-b). Therefore, the whole reaction process of ultraviolet radiation must be carried out in the ice-water bath.

2.3 Mechanical tests of synthesized hydrogels

2.3.1 Tensile test of synthesized hydrogels

For tensile test, all hydrogel samples were made in cylindrical tube mold with length of 70 mm and diameter of 4.6 mm. The hydrogel samples were test by INSTRON 5969 instrument (USA) immediately after been pushed out from the mold. Test conditions are listed below: loading speed was 100 mm min^{-1}, initial gauge length was 15 mm, load cell was 100 N and tested at room temperature of 20℃. To avoid the hydrogel samples sliding when tested, a thin layer soft paper was pasted onto the clamps before tested.

The tensile stress can be calculated from the applied force (F) divided by the cross-sectional area (A) in real-time during the stretching process, i.e., stress = F/A. The cross-sectional area A is defined as $A = A_0 \times L_0/L$, where A_0, L_0 and L refers to the initial cross-sectional area, the initial gauge length, and the real-time length of the hydrogel samples in the loading process.

For the recycle tensile test, the test conditions are listed below: the loading speed is 100 mm·min^{-1} while the unloading speed is 150 mm·min^{-1} and the initial gauge length is also kept at 15 mm.

For all these tensile and recycle tensile tests, each hydrogel samples were tested at least 3 times and the average value was adopted (as shown in table 2).

2.3.2 Compressive test of the synthesized hydrogels

For the compression tests, the compressive stress of hydrogel samples was achieved by the stress at the deformation of 90%. The test conditions are listed as below: initial height was 5

mm, compression speed was 10 mm·min^{-1} and tested at room temperature of 20℃

For all these compressive tests, each hydrogel samples were tested at least 3 times and the average value was adopted.

2.4 Swelling behaviors of the synthesized hydrogels

The equilibrium swelling ratios (ESR) test was conducted after the prepared hydrogel samples were immersed into DI water at room temperature for two weeks, changing water three times a day.

Firstly, a given amount of dried hydrogel samples were put into different pH value PBS solutions for 24 h at room temperature until their weight do not change anymore. Secondly, the swollen hydrogels were taken out and wiped with filter paper to remove their surface water before weighted. ESR values could be calculated by the following formula:

$$\mathrm{ESR} = (\mathrm{W_e} - \mathrm{W_d})/\mathrm{W_d} \quad (1)$$

where, $\mathrm{W_e}$ and $\mathrm{W_d}$ stands for the weight of the equilibrium and dried hydrogel samples, respectively. So the ESR-pH value curves were achieved.

For the swelling behaviors of hydorgel samples in different temperature deionized water or concentration of NaCl solutions, a given weight of swollen hydrogels (weight percent 100%) were put into the different temperature deionized water or concentration of NaCl solution for 24 h until their weight didn't change anymore. Then the hyrogel samples were taken out and their surface water was removed before weighted. Furthermore, we obtained the weight percent-temperature and weight percent-NaCl concentration curves of these hydrogel samples.

For all the above tests, each hydrogel samples were reproduced at least three times.

2.5 Conductive behaviors of hydrogel samples under recycle strain

The voltage applied to both ends of hydrogel sample is 1 V, which is provided by electrochemical workstation. The specified conditions are below: for tensile recycle test, the distance between upper and lower clamps is 10 mm, the width and thickness of samples are 5 mm and 1.5 mm, respectively; For the compressive test, the height between two rounded platens is 6 mm, the diameter of hydrogel sample is 4.6 mm, and the moving speed of the platens is 10 $mm \cdot min^{-1}$. It is necessary to mention that after the hydrogel sample was connected into the circuit, until the current in the whole circuit is stable, it is the time to test the resistance change rate of the hydrogel samples in the recycle stretching and compressing progress.

According to the applied voltage (1 V) on ends of the above round hydrogel sample and the current in the circuit ($1.18 \cdot 10^{-4}$ A), the conductivity of synthesized hydrogel sample is about $2.56 \cdot 10^{-2}$ S/m. After immersed in DI water for three days (change water three times a day), their conductivity is about $3.01 \cdot 10^{-5}$ S/m.

2.6 Thermo-sensitive behaviors of designed bilayer structure hydrogel actuator

The test conditions are listed as below: the length of one layer hydrogel is about 60 mm, width is about 10 mm, and thickness are about 1 mm, 1.5 mm or 2 mm respectively (No special instruction, the thickness is 1 mm.), water bath temperature is 37°C in Fig.11a-e, and 50°C in Fig.11f. Besides, all the images are taken after the hydrogel samples were immersed in water bath in 5 seconds.

2.7 NIR-light responsive behaviors of bilayer structure hydrogel actuator

After the obtained bilayer structure hydrogel sample was taken out from the mold, it was used to do the NIR-light responsive property immediately. The testing conditions are listed below: the current intensity of near infrared laser is 1.2 A, the area of light source is 3 mm·2 mm, the distance from light source to sample is 15 CM and the irradiation time is 25 s. Besides, the width of hydrogel bilayer is about 3 mm, the thickness is about 2 mm, and the length is about 60 mm.

3 Results and discussion

3.1 Raman spectra

The Raman spectra of GO, CPH, CMCTs and CGPH can be seen from Fig. 2a. GO nanosheets own two characteristic peaks at 1350 and 1590 cm^{-1}, but CMCTs and CPH only have two weak typical peaks at 1277, 1446 cm^{-1} and 1259, 1430 cm^{-1} respectively[35]. Generally speaking, intensity ratio of GO (I_D/I_G) is 0.8, however, the I_D/I_G ratio in CGPH is 1.05. The primarily reason for this phenomenon is that part of the carboxyl groups on GO nanosheets have already reacted with amino groups of CMCTs, which results in more defects on the surface of GO, and at the same time, G band of GO nanosheets shifts to 1600 cm^{-1} in CGPH[36]. By comparing the curves of $C_{25}G_{0.103}P_{5\text{-}0.467}H$, $C_{25}G_{0.103}P_{7.5\text{-}0.467}H$ and $C_{25}G_{0.103}P_{15\text{-}0.467}H$, it can be clearly seen that with the incorporation of more EDC, the I_D/I_G ratio increases greatly, indicating that more defects are formed on GO nanosheets. In Fig.2a, although the surface of GO nanosheets in synthesized hydrogel was destroyed in some extent,

Raman pattern remains, which implies that the overall graphitic structure of GO was reserved[37].

3.2 XRD spectrum

XRD spectra of GO, CMCTs and CGPH are displayed in Fig. 2b. GO nanosheets have a lower characteristic diffraction peak around 2θ=10.18°, associated with an interlayer distance about 0.877 nm, which is in consistent with the literature reported before[38]. The typical peak of CMCTs is at 2θ=20.5º. From the curves of CGPH, it is evidently to find that there is no peak appear at 2θ=10.18º and 20.5°, which reveals that both GO nanosheets and CMCTs polymer chains have good dispersibility in the hydrogels[25]. With the addition of more BAC, EDC, CMCTs or GO, the sharp degree of peaks of the prepared hydrogel samples at 2θ=8.15° and 22.13°increases. The primary reason for this phenomenon may be that with the incorporation of more BAC or EDC, the crosslink degree between the polymer chains increases and the distance between them decreases, resulting in stronger intensity of peaks; with more CMCTs or GO added in, the physical interaction between polymer chains (CMCTs and PNIPAm) and GO increases, leading to the stronger peak intensity[39,40]. Besides, with the addition of more CMCTs, the characteristic peak of CGPH moves to the higher degree direction. The primarily reason may be that the distance between polymer chains decreases with the content of CMCTs increases. Furthermore, from Bragg equation[41], it can be inferred that as the distance decreases, the 2θ value should be increased correspondingly, which is in line with the trend in Fig. 2b.

3.3 Mechanical properties of synthesized hydrogels

3.3.1 Tensile test of synthesized hydrogels

In this work, we have systematically investigated the essential factors on the tensile property of synthesized hydrogels, such as the concentration of BAC, EDC, CMCTs and GO. The image of tensile test process of prepared hydrogel sample was shown in Fig.S3c, and from which we can clearly see that there are plenty of bamboo-like joints on hydrogel samples when stretched. This phenomenon signifies that double network structure has already been formed in the hydrogel[42]. As can be seen from Fig. 3a-d, in general, with the incorporation of more BAC, EDC, CMCTs or GO, the breaking elongation decreases, the strain hardening phenomenon appears at smaller strain and simultaneously the elastic modulus (ε_t=10-20 %) increases. However, the breaking tensile strength increases at first and then decreases, which can be clearly seen in Table 2. Following reason may illuminate this phenomena: with the addition of more BAC, EDC or CMCTs, the crosslink density of the hydrogel sample increases, leading to shorter inter-crosslinked chain length, lower failure strain, higher elastic modulus and stronger tensile property[43]; but when the crosslink density increase too much, more irregular structure may exist in the hydrogels, results in more stress-concentration points and lower breaking tensile strength.

When GO content is too low, the distance between CMCTs polymer chains is small, resulting in fast reaction speed and more irregular structure in the hydrogel, so the failure strain and breaking tensile strength is lower. With GO content increases, the reaction speed decreases, more uniformly structure hydrogels were obtained, leading to higher failure strain and tensile stress. However, when GO content is continue increases, GO nanosheets may

absorb most of the UV light, leading to lower decomposition efficiency of photo-initiator (I2959) and uneven polymer network structure in the hydrogel. What's more, the breaking elongation and failure strength are decrease. From the above description, it is noticed to confirm that the content of BAC, EDC, CMCTs and GO has critical effect on the tensile properties of synthesized hydrogels and the optimal hydrogel owns the highest tensile strength of 1.046 MPa at the strain of 1286%, which is similar to the strength of the previous reported NC PNIPAm hydrogels[31] (about 1.05 MPa) and higher than DC NC PNIPAm hydroels[24] (about 770 kPa).

3.3.2 Energy dissipation mechanism and recoverable property

So as to understand the energy dissipation mechanism of synthesized hydrogel more clearly, recycle tensile tests were carried out and the toughness of the hydrogel is calculated by the area covered by the stress-strain curve at the breaking point[44]. As shown in Fig.4a, three times continuous loading-unloading recycle tensile test was conducted on the optimum hydrogel sample, with the end strain from 200 % to 600 %. Toughness of the prepared hydrogel increases as the end strain increase, which indicates that polymer networks, especially the physical networks, are destroyed seriously at a higher tensile strain. By contrasting the three closed areas, the difference between adjacent curves increases remarkably with the end strain increases, which represents the trend of damage degree in each loading process[45].

In order to understand the recoverability of manufactured hydrogel samples, the different time interval loading-unloading recycle tests were conducted, as displayed in Fig.4b. Comparing with the original recycle curve, toughness of the other three curves decreases

extensively, are 6.4 %, 45 % and 51.2 % of the original, respectively. This phenomenon suggests that polymer netwoks in the hydrogel sample was destroyed enormously and could not recovered in a short time. The unrecoverable toughness mainly corresponds to the destroyed rigid polymer netwoks and the recoverable toughness is primarily referred to physical interaction between the polymer chains[46].

3.3.3 Compressive test of synthesized hydrogels

The compressive stress-strain curves of synthesized hydrogel samples with different content of BAC, EDC, CMCTs or GO are shown in Fig.5a-d. As the content of BAC, EDC or CMCTs increases, both compressive stress (at the deformation of 90 %) and compressive modulus (ε_c = 5 – 10 %) increase (as displayed in Table 2). The mainly reason might be that with the addition of more BAC or EDC, the crosslink points in the hydrogel increases, resulting in higher compressive modulus value and higher compressive stress; with the incorporation of more CMCTs, the reaction speed between CMCTs polymer chains increases, lead to higher crosslink density and mechanical property (compressive stress and modulus)[47]. However, with the addition of more GO nanosheets, the distance between the polymer chains increases, making the crosslink density decrease and resulting in lower mechanical property (compressive stress and modulus).

3.4 SEM morphology

As exhibited in Fig. 6a-k, it is evidently to see that pore size of the synthesized hydrogels is generally at micrometer level. As illustrated in Fig.6 a-f, with the addition of more BAC or EDC, pores become more smaller and denser, and the largest pore size decreases from 13 to

6μm, and 12 to 8μm, respectively, which is mainly attributed to more crosslink points and higher density in the prepared hydrogels. With more CMCTs added in, there are plenty of obvious cotton-shaped connectors in the bigger pores of synthesized hydrogels, which leads to large amounts of smaller pores in the bigger holes, and the largest pore size decreases from 12 to 8μm. Interpretation of this phenomenon may be that physical interaction and crosslink degree between the polymer chains increase greatly with the addition of more CMCTs[48].

As displayed in Fig.6 j,h,k, with the incorporation of more GO nanosheets, pore size of the fabricated hydrogels increases from 8 to 14μm at first, and then decreases to 10μm. Appropriate interpretation for this phenomenon might be that with more GO nanosheets added in, the distance between polymer chains increases at first; however, as the GO content continue increases, the more regular and dense arrangement of GO nanosheets leads to the decrease of pore size[25].

3.5 Swelling behaviors of synthesized hydrogels

3.5.1 Swelling behaviors of synthesized hydrogels in different pH value solutions

Swelling behaviors of prepared CGPH in different pH value PBS solutions at room temperature was shown in Fig.7. In general, as pH value increases, ESR of the synthesized hydrogels increases fast at first and then decreases greatly. When pH=1, there are plenty of hydrogen bonds in the hydrogels, results in low ESR values. When pH=2, although the hydrogen bonds decreases to some extent, there are still large amounts of $–NH_3^+$ in the hydrogel, leading to higher ESR values[49]. As pH value increases to 3, some of the $-NH_3^+$ ions decrease, making the repulsion force between them decreases and leading to a relative

smaller ESR value. When pH value is between 4 and 7, large amounts of $-NH_3^+$ ions disappear, which results in lower ESR value; but hydrogen bonds are decreased remarkably simultaneously, leading to high ESR value. Since the latter factor plays the major role in swelling behaviors, ESR values increase a little. With pH≥8, osmotic pressure is higher in the solution, which makes the ESR values decrease dramatically[50].

As displays in Fig.7a-b, with the addition of more BAC or EDC, the denser crosslink points and shorter polymer chains in hydrogels result in smaller ESR value in total. With more CMCTs added in, as exhibited in Fig. 7c, ESR values decrease when pH≤6 but increase when pH≥8. The explanation might be that as the content of CMCTs increases, there are more $-COO^-$ ions in the hydrogels when pH≥8, resulting in stronger repulsion interaction between the polymer chains and higher ESR values. As shown in Fig.7d, with the incorporation of more GO nanosheets, when pH≤3 and pH≥8 , ESR values increase at first and then decrease. The interpretaion for this phenonmen may that with the addition of little GO nanosheets, the inner regular polymer structure destroyed to some extent , so the ESR vlaue increases at first when pH = 2 (repulsion force is more stronger at this time) and decreases when pH≥ 8 (osmotic pressure playing the key role in shrinking the hydrogel volume); however, as the GO content continue increases, the inner polyemer networks are more regular and the crosslink density increases more strikingly, leading to smaller (pH=2) and higher (pH=8) ESR values, respectively[25].

3.5.2 Swelling behaviors of synthesized hydrogels in different temperature solutions

Swelling behaviors of the fabricated CGPH hydrogel samples at different temperature in DI water bath is shown in Fig.8. As the temperature increases, weight of the hydrogel samples

decreases, especially dramatically decreased near the volume phase transition temperature (VPTT), which is mainly attributed to the hydrophilic-hydrophobic conversion of groups in hydrogel samples. It is obviously to see that at one fixed temperature, weight percent increases with the addition of more BAC, EDC, CMCTs or GO. The proper interpretation for this phenomenon may be that as the above factors' content increases, the cross-link density in hydrogel samples increases[51] (as shown in Fig.6), resulting in higher weight percent.

3.5.3 Swelling behaviors of synthesized hydrogels in different concentration NaCl solutions

Weight percent of the prepared hydrogel samples in different NaCl concentration was displayed in Fig.9. It is obviously to see that as the concentration of NaCl increases, weight percent of all the hydrogel samples decreases at first and then increases to some extent. The possible reason may be that as the concentration of NaCl increases, the osmotic pressure difference (between inner and out of the polymer chains) is much more different, leads to the shrinkage of polymer chains and the shorter volume of hydrogels. However, with the further increase of NaCl concentration (>2M), the osmotic pressure inside the solution increases greatly and more ionic groups are running into the polymer chains, resulting in larger volume of hydrogel samples[52].

In addition, with the addition of more BAC, EDC, CMCTs or GO, the maximum variation of weight percent (NaCl concentration from 0.5 to 4M) decreases in general. The primary interpretation may be that crosslink density in hydrogels increases with the addition of more the above mentioned factors, resulting in the shorter shrink volume range in total.

In general, based on pH-, thermo- or NaCl concentration- sensitive properties, these synthesized hydrogel samples can be used as the pH- and temperature- sensitive controllers

and chemical valves.

3.6 Conductive behaviors of hydrogel samples under recycle strain

Considering both PNIPAm and CMCTs polymer chains are polyelectrolyte materials[53] and there are also lots of MES molecules in the hydrogel samples, so the prepared hydrogel samples own good ionic conductivity (their conductivity is about $2.56 \cdot 10^{-2}$ S/m, as shown in section 2.5). As shown in Fig.S4, when synthesized hydrogel sample was insert into the circuitry, LED light emit light, which demonstrates that the obtained hydrogel possess good conductivity. In order to disclose the feasibility of the designed hydrogel as strain biosensor devices[12], the electric current of optimal hydrogel sample under different recycle tensile and compressive strain was recorded by electrochemical workstation at the voltage of 1 V. As exhibited in Fig.10, in the recycle elongation (a) and compression (b) process, the resistance change rate varies regularly at different tensile (150%, 300%) and compression strain (25%, 50%). The resistance change rate displays a quickly response to the variation of strain, suggesting that these hydrogels own good strain sensitivity. Elongation makes the resistance of hydrogel sample increase (as shown in Fig.S5, the brightness of LED lamp decreases when the tensile strain increases) while compression decrease. This excellent stable strain responsive property in resistance makes it an ideal material as strain-biosensor (deformation monitor) on highly flexible area, such as elbow or knee.

3.7 Thermo-sensitive behaviors of designed bilayer structure hydrogel actuator

At present, there are many reports about the design of bilayer thermo-sensitive bending actuators, but they mainly focus on single-network structure inorganic NC thermo-sensitive

hydrogels, which are prepared by controlling the concentration of nanoparticles in the two-layer hydrogels to change their internal crosslink density[54]. The adjustable factors are limited and the acid-alkali resistance of these inorganic nanocomposite hydrogels is usually poor. In theory, the chemical cross-linked double network hydrogel has higher mechanical property and better acid-alkali resistance than nanocomposite hydrogel, so we attempt to design the chemical cross-linked double network structure thermal-/NIR- responsive bilayer hydrogel actuator. To the best of our knowledge, it is the first time to synthesize the double network structure thermal-/NIR- responsive bilayer actuator.

As shown in Fig.11a-c, with the addition of more BAC, EDC or CMCTs in one layer (compared with another), the fabricated bilayer hydrogel sample bends to the high content layer side when it was put into the water bath. The reason for this phenomenon is that higher content of BAC, EDC or CMCTs results in more crosslink points, leading to stronger bending ability when put into the 37°C water bath, so the bilayer hydrogel sample bends to the higher crosslink density side[55]. However, as the content of GO increases, as displays in Fig.11d, the bilayer hydrogel sample firstly bends to the higher GO content side, and then when GO content is continue increases, it bends to the lower content side. The possible interpretation is that, when GO content is in a suitable range, the hydrogel sample's inner crosslink density increases as the GO content increases[24]; however, with the GO content continue increases, the crosslink density the hydrogel sample may decrease (as interpreted in 2.2.3), leading to bending to the lower GO content side.

With the thickness of one layer hydrogel increases, the bending degree decreases with the thickness increases, which is mainly attributed to that the higher thickness corresponds to

higher weight, making the bending degree decrease. Finally, we try to prepare the cross-shaped bilayer hydrogel sample with the same thickness on both sides (1 mm) using the same components as in Fig.11e. When the hydrogel sample was put into the water bath with the temperature of 50℃, the claw-shaped shrinkage of the hydrogel sample can be clearly seen in Fig. 3-11f. This excellent thermo-responsive bending property provides these bilayer hydrogel samples with tremendous potential use in remote thermo-control actuators in future.

3.8 NIR-light responsive behaviors of the bilayer structure hydrogel actuator

Bending images of the synthesized bilayer hydrogel samples with different component under 808 nm IR light were shown in Fig.12. For the $C_{22.5}G_{0}P_{7.5\text{-}0.266}$/$C_{22.5}G_{0.103}P_{7.5\text{-}0.266}$ bilayer hydrogel, as exhibited in Fig.12a, it bends to the side containing graphene oxide when the near infrared laser light is on (about 1.5mm away from its original vertical position). For the $C_{25}G_{0.103}P_{5\text{-}0.266}$/ $C_{25}G_{0.103}P_{12.5\text{-}0.266}$ bilayer hydrogel sample (as shown in Fig.12b), it bends to the side with higher crosslink density when the laser is on (about 1.5mm away from its original vertical position), which was in line with the temperature-responsive bending property in Fig.11. Owing to this good NIR- responsive property, bilayer structure hydrogel sample could be potential used as the remote NIR- controller (actuator) in the dangerous places in future.

4 Conclusion

In conclusion, we designed a novel biocompatible mechanical strong stretchable conductive near-infrared light-/thermal-/pH-/ionic concentration- responsive CMCTs/GO/PNIPAm nanocomposite double network hydrogel by a facile one-pot *in situ* free radical polymerization, which is initiated by UV light, using EDC and BAC as cross-linkers to

crosslink CMCTs/GO and PNIPAm polymer chains, respectively. A suitable concentration of GO plays a key role in protecting disulfide bonds in BAC and preparing flexible and effective cross-linking PNIPAm polymer network in the obtained hydrogels. When the concentration of CMCTs, GO, EDC and BAC is 22.50, 0.10, 7.50 and 0.47 mg/mL, respectively, the CMCTs/GO/PNIPAm hydrogel exhibits the highest tensile strength of 1.05 MPa at the breaking strain of 1286 % and a corresponding compressive stress of 2.37 MPa at the deformation of 90 %. These synthesized hydrogels could absorb plenty of energy under the elongation process, but just only recover to its original sample's 51.20% at the room temperature after unloaded in 15 min. Furthermore, these synthesized hydrogels have an obvious pH-/temperature-/ionic concentration- responsive properties depending on the concentration of the above mentioned factors. In addition, we attempt to design a novel thermal-/NIR- responsive double network structure bilayer actuators and their bending degree could be adjusted by the inner crosslink density, which have the potential use as remote control actuator in dangerous places. At last, resistance of these conductive fabricated hydrogel changes evenly with the variation of elongation and compressive strain, which makes it a candidate material as healthcare biosensors in future.

Declaration of Conflicting Interests

The author(s) declared no potential conflicts of interest with respect to the research, authorship, and/or publication of this article.

Acknowledgement

This work was financially supported by Shanghai International S&T Cooperation Fund (16160731302), Natural Science Foundation of China (No.51473031) and Nature Science Foundation of Shanghai (Grant No. 17ZR1401100).

References

1. Guragain S, Bastakoti BP, Malgras V, Nakashima K, Yamauchi Y. Multi-Stimuli-Responsive Polymeric Materials. Chem Eur J. 2015;21(38):13164-74.

2. Miyamoto N, Shintate M, Ikeda S, Hoshida Y, Yamauchi Y, Motokawa R, et al. Liquid crystalline inorganic nanosheets for facile synthesis of polymer hydrogels with anisotropies in structure, optical property, swelling/deswelling, and ion transport/fixation. Chem Commun, 2013;49(11):1082-4.

3. Chen Y, Wang H, Yu J, Wang Y, Zhu J, Hu Z. Mechanically strong and pH-responsive carboxymethyl chitosan/graphene oxide/polyacrylamide nanocomposite hydrogels with fast recoverability. J Biomat Sci-Polym Ed, 2017;28(16):1899-917.

4. Ter Schiphorst J, Van Den Broek M, De Koning T, Murphy J, Schenning A, Esteves A. Dual light and temperature responsive cotton fabric functionalized with a surface-grafted spiropyran–NIPAAm-hydrogel. J Mater Chem A, 2016;4(22):8676-81.

5. Yang L, Wang Z, Fei G, Xia H. Polydopamine Particles Reinforced Poly (vinyl alcohol) Hydrogel with NIR Light Triggered Shape Memory and Self-Healing Capability. Macromol Rapid Comm, 2017;38(23):1700421.

6. Yang C, Liu Z, Chen C, Shi K, Zhang L, Ju X-J, et al. Reduced Graphene Oxide-Containing Smart Hydrogels with Excellent Electro-Response and Mechanical Properties for Soft Actuators. ACS Appl Mater Inter, 2017;9(18):15758-67.

7. Cirillo G, Curcio M, Spizzirri UG, Vittorio O, Tucci P, Picci N, et al. Carbon nanotubes hybrid hydrogels for electrically tunable release of Curcumin. Eur Polym J, 2017;90:1-12.

8. Hu K, Sun J, Guo Z, Wang P, Chen Q, Ma M, et al. A Novel Magnetic Hydrogel with Aligned Magnetic Colloidal Assemblies Showing Controllable Enhancement of Magnetothermal Effect in the Presence of Alternating Magnetic Field. Adv Mater, 2015;27(15):2507-14.

9. Wang P, Sun J, Lou Z, Fan F, Hu K, Sun Y, et al. Assembly-Induced Thermogenesis of Gold Nanoparticles in the Presence of Alternating Magnetic Field for Controllable Drug Release of Hydrogel. Adv Mater, 2016;28(48):10801-8.

10. Ma Y, Zhang Y, Wu B, Sun W, Li Z, Sun J. Polyelectrolyte multilayer films for building energetic walking devices. Angewandte Chemie. 2011;123(28):6378-81.

11. Wei Q-B, Luo Y-L, Fu F, Zhang Y-Q, Ma R-X. Synthesis, characterization, and swelling kinetics of pH-responsive and temperature-responsive carboxymethyl chitosan/polyacrylamide hydrogels. J Appl Polym Sci, 2013;129(2):806-14.

12. Chen F, Lu S, Zhu L, Tang Z, Wang Q, Qin G, et al. Conductive regenerated silk-fibroin-based hydrogels with integrated high mechanical performances. J Mater Chem B. 2019; 7:1708-1715.

13. Ionov L. Hydrogel-based actuators: possibilities and limitations. Materials Today. 2014;17(10):494-503.

14. Patel KK, Gade S, Anjum MM, Singh SK, Maiti P, Agrawal AK, et al. Effect of penetration enhancers and amorphization on transdermal permeation flux of raloxifene-encapsulated solid lipid nanoparticles: an ex vivo study on human skin. Appl Nanosci, 2019;9(6):1383-94.

15. Islam MR, Li X, Smyth K, Serpe MJ. Polymer-based muscle expansion and contraction. Angew Chem Int Ed Engl. 2013;52(39):10330-3.

16. Iamsaard S, Aßhoff SJ, Matt B, Kudernac T, Cornelissen JJ, Fletcher SP, et al. Conversion of light into macroscopic helical motion. Nat Chem, 2014;6(3):229-34.

17. Hoffman AS. Hydrogels for biomedical applications. Adv Drug Deliver Rev, 2012;64:18-23.

18. Cui W, Zhang Z-J, Li H, Zhu L-M, Liu H, Ran R. Robust dual physically cross-linked hydrogels with unique self-reinforcing behavior and improved dye adsorption capacity. RSC Adv, 2015;5(65):52966-77.

19. Feng Z, Zuo H, Gao W, Ning N, Tian M, Zhang L. A Robust, Self-Healable, and Shape Memory Supramolecular Hydrogel by Multiple Hydrogen Bonding Interactions. Macromol rapid comm. 2018;39(20):1800138.

20. Di X, Kang Y, Li F, Yao R, Chen Q, Hang C, et al. Poly (N-isopropylacrylamide)/Polydopamine/Clay Nanocomposite Hydrogels with Stretchability, Conductivity, and Light/Thermo Dual Responsive Bending and Adhesive Properties. Colloid Surfaces B: Biointerfaces. 2019; 177:149-159.

21. Chen Y, Kang S, Yu J, Wang Y, Zhu J, Hu Z. Tough robust dual responsive nanocomposite hydrogel as controlled drug delivery carrier of asprin. Journal Mech Behav

Biomed, 2019;92:179-187.

22. Chen H, Chen Q, Hu R, Wang H, Newby B-mZ, Chang Y, et al. Mechanically strong hybrid double network hydrogels with antifouling properties. J Mater Chem B, 2015;3(27):5426-35.

23. Gao G, Du G, Sun Y, Fu J. Self-healable, tough, and ultrastretchable nanocomposite hydrogels based on reversible polyacrylamide/montmorillonite adsorption. ACS Appl Mater Interf, 2015;7(8):5029-37.

24. Shi K, Liu Z, Wei Y-Y, Wang W, Ju X-J, Xie R, et al. Near-infrared light-responsive poly (N-isopropylacrylamide)/graphene oxide nanocomposite hydrogels with ultrahigh tensibility. ACS Appl Mater Interf, 2015;7(49):27289-98.

25. Huang S, Shen J, Li N, Ye M. Dual pH-and temperature-responsive hydrogels with extraordinary swelling/deswelling behavior and enhanced mechanical performances. J Appl Polym Sci, 2015;132(9):41530-41538.

26. Chen Y, Peng C, Lu Y, Liu W, Xu W. Responsiveness and release characteristic of semi-IPN hydrogels consisting of nano-Sized clay crosslinked poly (dimethylaminoethyl methacrylate) and linear carboxymethyl chitosan. J Nanosci Nanotechno, 2015;15(1):164-71.

27. Chen Y, Song G, Yu J, Wang Y, Zhu J, Hu Z. Mechanically strong dual responsive nanocomposite double network hydrogel for controlled drug release of asprin. J Mech Behav Biomed, 2018;82:61-9.

28. He G, Chen X, Yin Y, Cai W, Ke W, Kong Y, et al. Preparation and antibacterial properties of O-carboxymethyl chitosan/lincomycin hydrogels. J Biomat Sci-Polym E, 2016;27(4):370-84.

29. Gorgieva S, Kokol V. Preparation, characterization, and in vitro enzymatic degradation of chitosan-gelatine hydrogel scaffolds as potential biomaterials. J Biomed Mater Res A, 2012;100(7):1655-67.

30. Zhang E, Wang T, Lian C, Sun W, Liu X, Tong Z. Robust and thermo-response graphene–PNIPAm hybrid hydrogels reinforced by hectorite clay. Carbon, 2013;62:117-26.

31. Qin H, Zhang T, Li H-N, Cong H-P, Antonietti M, Yu S-H. Dynamic Au-thiolate interaction induced rapid self-healing nanocomposite hydrogels with remarkable mechanical behaviors. Chem. 2017;3(4):691-705.

32. Oh JH, Hong SY, Park H, Jin SW, Jeong YR, Oh SY, et al. Fabrication of high-sensitivity skin-attachable temperature sensors with bioinspired microstructured adhesive. ACS Appl Mater Interf, 2018;10(8):7263-70.

33. Chen Y, Qiao S, Yu J, Wang Y, Zhu J, Hu Z, editors. A novel dual responsive nanocomposite double network hydrogel with good mechanical property. IOP Conference Series: Earth and Environmental Science; 2018: IOP Publishing.

34. Loebel C, D'Este M, Alini M, Zenobi-Wong M, Eglin D. Precise tailoring of tyramine-based hyaluronan hydrogel properties using DMTMM conjugation. Carbohydr polym, 2015;115:325-33.

35. Lin C, Liu Y-T, Xie X-M. Improved mechanical properties of graphene oxide/poly (ethylene oxide) nanocomposites by dynamic interfacial interaction of coordination. Aust J Chem, 2014;67(1):121-6.

36. Ruan J, Wang X, Yu Z, Wang Z, Xie Q, Zhang D, et al. Enhanced Physiochemical and Mechanical Performance of Chitosan-Grafted Graphene Oxide for Superior Osteoinductivity.

Adv Funct Mater, 2016;26(7):1085-97.

37. Park S, Lee K-S, Bozoklu G, Cai W, Nguyen ST, Ruoff RS. Graphene oxide papers modified by divalent ions—enhancing mechanical properties via chemical cross-linking. ACS Nano. 2008;2(3):572-8.

38. Justin R, Chen B. Characterisation and drug release performance of biodegradable chitosan–graphene oxide nanocomposites. Carbohyd Polym, 2014;103:70-80.

39. Han D, Yan L. Supramolecular hydrogel of chitosan in the presence of graphene oxide nanosheets as 2D cross-linkers. ACS Sustain Chem Eng, 2014;2(2):296-300.

40. Sun J-Y, Zhao X, Illeperuma WR, Chaudhuri O, Oh KH, Mooney DJ, et al. Highly stretchable and tough hydrogels. Nature. 2012;489(7414):133-6.

41. Zhong M, Liu Y-T, Xie X-M. Self-healable, super tough graphene oxide–poly (acrylic acid) nanocomposite hydrogels facilitated by dual cross-linking effects through dynamic ionic interactions. J Mater Chem B, 2015;3(19):4001-8.

42. Gong JP. Why are double network hydrogels so tough? Soft Matter. 2010;6(12):2583-90.

43. Chen Q, Zhu L, Zhao C, Wang Q, Zheng J. A robust, one-pot synthesis of highly mechanical and recoverable double network hydrogels using thermoreversible sol-gel polysaccharide. Adv Mater, 2013;25(30):4171-6.

44. Hu Y, Du Z, Deng X, Wang T, Yang Z, Zhou W, et al. Dual physically cross-linked hydrogels with high stretchability, toughness, and good self-recoverability. Macromolecules. 2016;49(15):5660-8.

45. Chen Q, Zhu L, Huang L, Chen H, Xu K, Tan Y, et al. Fracture of the physically cross-linked first network in hybrid double network hydrogels. Macromolecules.

2014;47(6):2140-8.

46. Lu X, Chan CY, Lee KI, Ng PF, Fei B, Xin JH, et al. Super-tough and thermo-healable hydrogel–promising for shape-memory absorbent fiber. J Mater Chem B, 2014;2(43):7631-8.

47. Chen Q, Chen H, Zhu L, Zheng J. Engineering of tough double network hydrogels. Macromol Chem Phys, 2016;217(9):1022-36.

48. Wei Q-B, Fu F, Zhang Y-Q, Tang L. Synthesis and characterization of pH-responsive carboxymethyl chitosan-g-polyacrylic acid hydrogels. J Polym Res, 2015;22(2):15.

49. Chen J, Sun J, Yang L, Zhang Q, Zhu H, Wu H, et al. Preparation and characterization of a novel IPN hydrogel memberane of poly (N-isopropylacrylamide)/carboxymethyl chitosan (PNIPAAM/CMCS). Radiat Phys Chem, 2007;76(8-9):1425-9.

50. Li Z, Shen J, Ma H, Lu X, Shi M, Li N, et al. Preparation and characterization of pH-and temperature-responsive hydrogels with surface-functionalized graphene oxide as the crosslinker. Soft Matter. 2012;8(11):3139-45.

51. Yao C, Liu Z, Yang C, Wang W, Ju X-J, Xie R, et al. Smart hydrogels with inhomogeneous structures assembled using nanoclay-cross-linked hydrogel subunits as building blocks. ACS Appl Mater Interf, 2016;8(33):21721-30.

52. Wei QB, Luo YL, Fu F, Zhang YQ, Ma RX. Synthesis, characterization, and swelling kinetics of pH-responsive and temperature-responsive carboxymethyl chitosan/polyacrylamide hydrogels. J Appl Polym Sci, 2013;129(2):806-14.

53. Wu J, Wu Z, Han S, Yang B-R, Gui X, Tao K, et al. Extremely Deformable, Transparent, and High-Performance Gas Sensor Based on Ionic Conductive Hydrogel. ACS Appl Mater Interf, 2018;11(2):2364-73.

54. Yao C, Liu Z, Yang C, Wang W, Ju XJ, Xie R, et al. Poly (N-isopropylacrylamide)-clay nanocomposite hydrogels with responsive bending property as temperature-controlled manipulators. Adv Funct Mater, 2015;25(20):2980-91.

55. Ma C, Lu W, Yang X, He J, Le X, Wang L, et al. Bioinspired anisotropic hydrogel actuators with on–off switchable and color-tunable fluorescence behaviors. Adv Funct Mater, 2018;28(7):1704568.

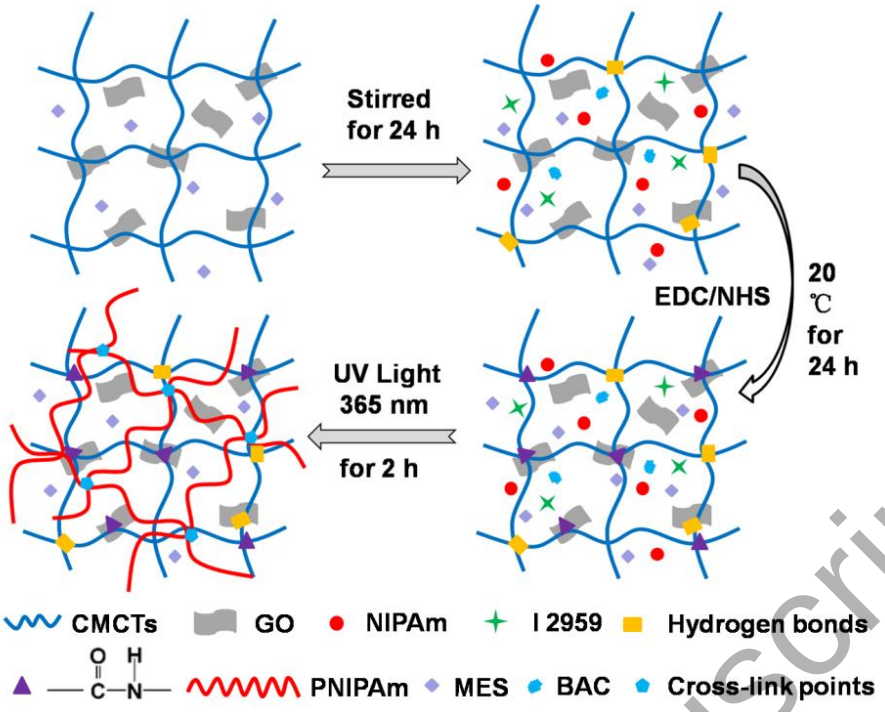

Fig. 1 The synthesis process of CMCTs/GO/PNIPAm NC DN hydrogels

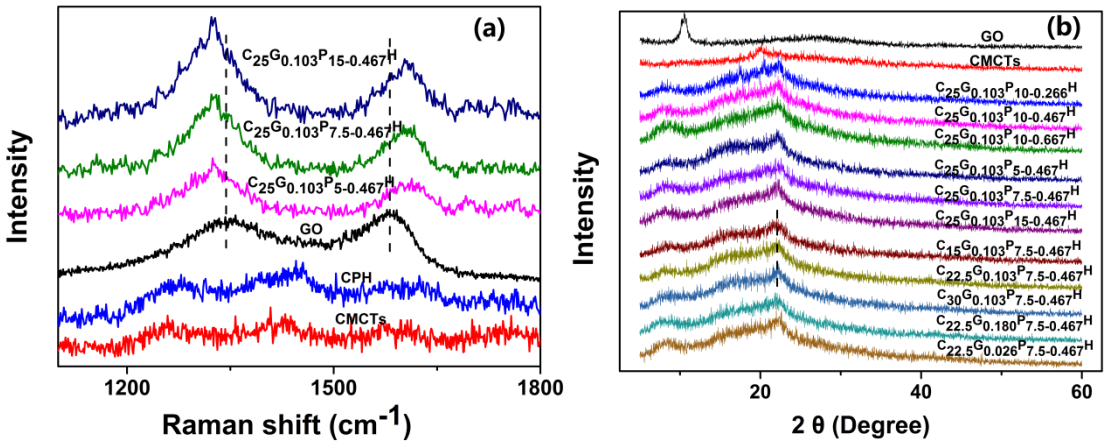

Fig. 2 (a) The Raman spectra of GO, CPH, CMCTs and CGPH, and (b) the XRD spectra of GO, CMCTs and CGPH

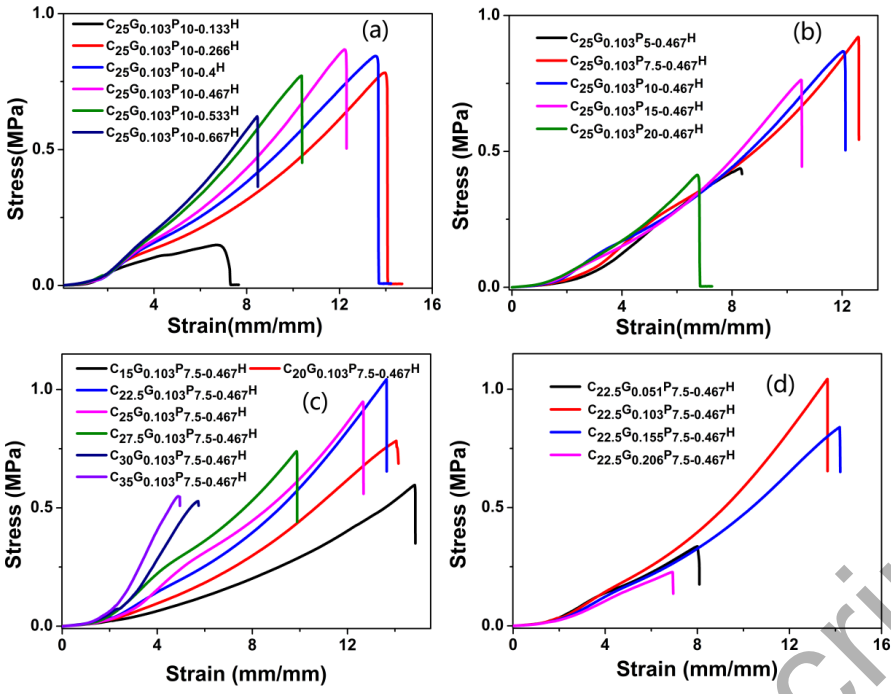

Fig. 3 The stress-strain curves of synthesized hydrogel samples with different content of (a) BAC, (b) EDC, (c) CMCTs and (d) GO

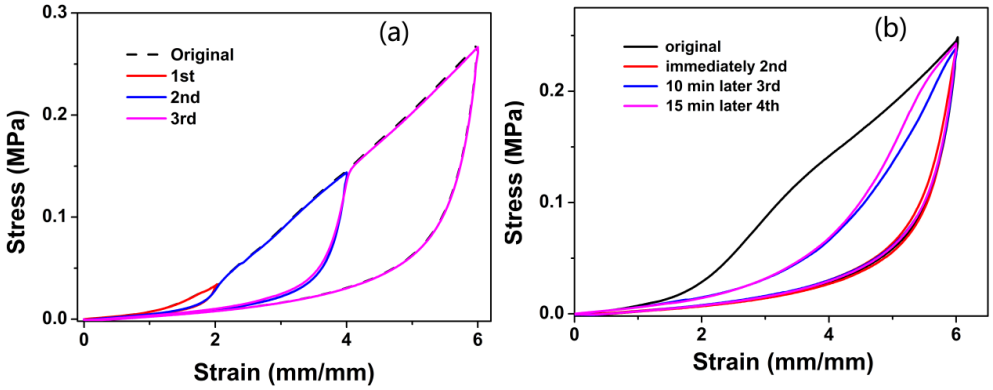

Fig. 4 The recycle stress-strain curves synthesized hydrogel samples (a) with different end strain and (b) at the same strain with different recovery time

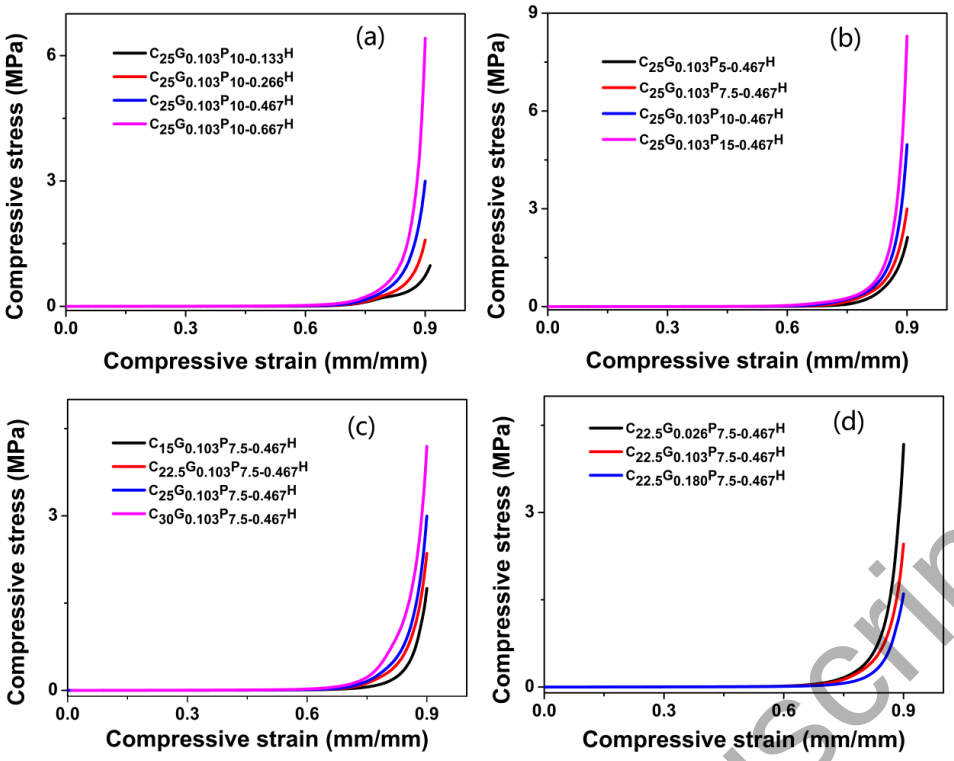

Fig. 5 The compressive stress-strain curves of synthesized hydrogel samples with different content of BAC, EDC, CMCTs and GO (ε_c = 90%)

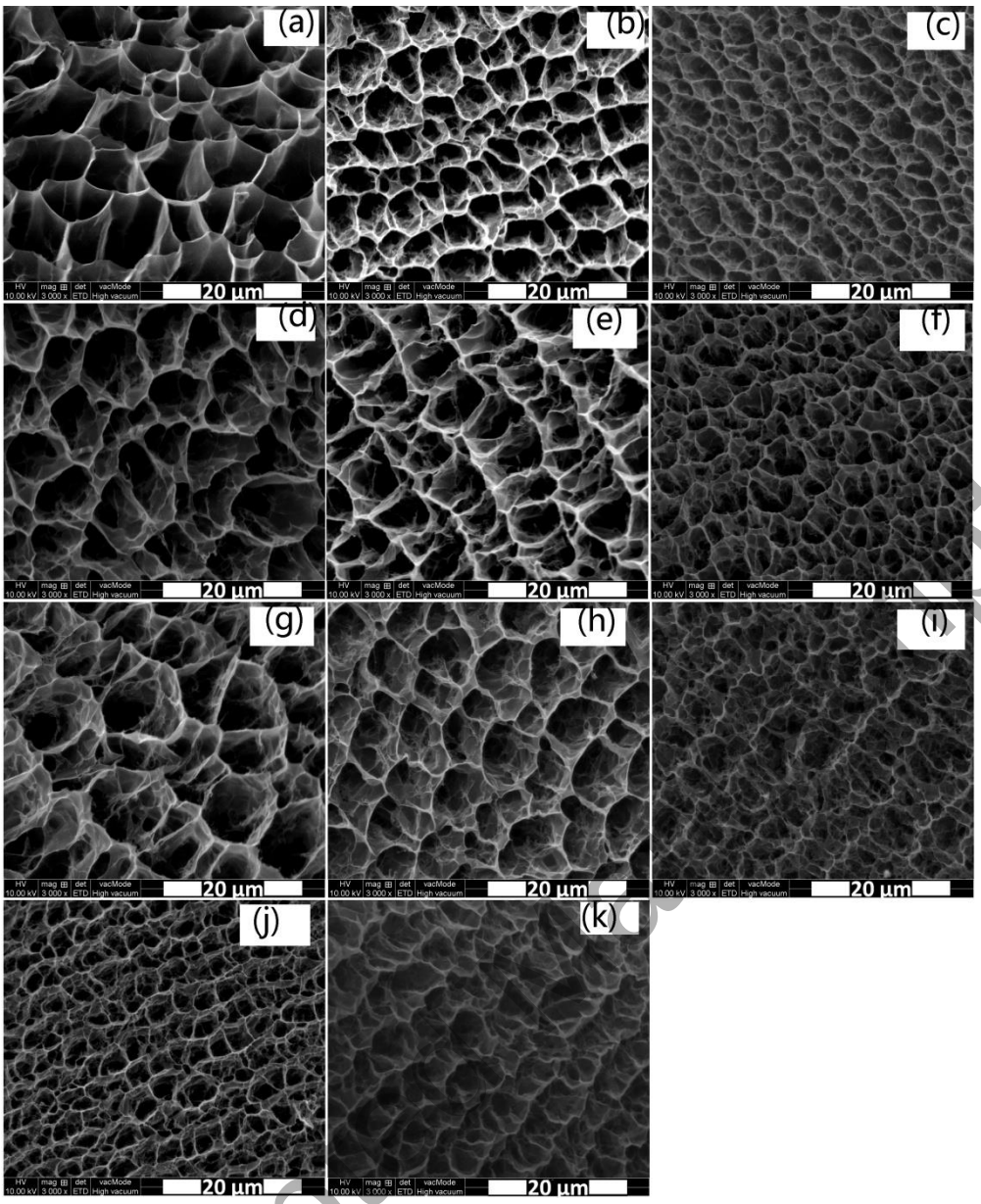

Fig. 6 The SEM image of synthesized hydrogel samples with different content of BAC，EDC，CMCTs and GO, （a）$C_{25}G_{0.103}P_{10\text{-}0.266}H$，（b）$C_{25}G_{0.103}P_{10\text{-}0.467}H$，（c）$C_{25}G_{0.103}P_{10\text{-}0.667}H$，（d）$C_{25}G_{0.103}P_{5\text{-}0.467}H$，（e）$C_{25}G_{0.103}P_{7.5\text{-}0.467}H$，（f）$C_{25}G_{0.103}P1_{5\text{-}0.467}H$，（g）$C_{15}G_{0.103}P_{15\text{-}0.467}H$，（h）$C_{22.5}G_{0.103}P_{15\text{-}0.467}H$，（i） $C_{30}G_{0.103}P_{15\text{-}0.467}H$，（j） $C_{22.5}G_{0.051}P_{15\text{-}0.467}H$，（k） $C_{22.5}G_{0.206}P_{15\text{-}0.467}H$

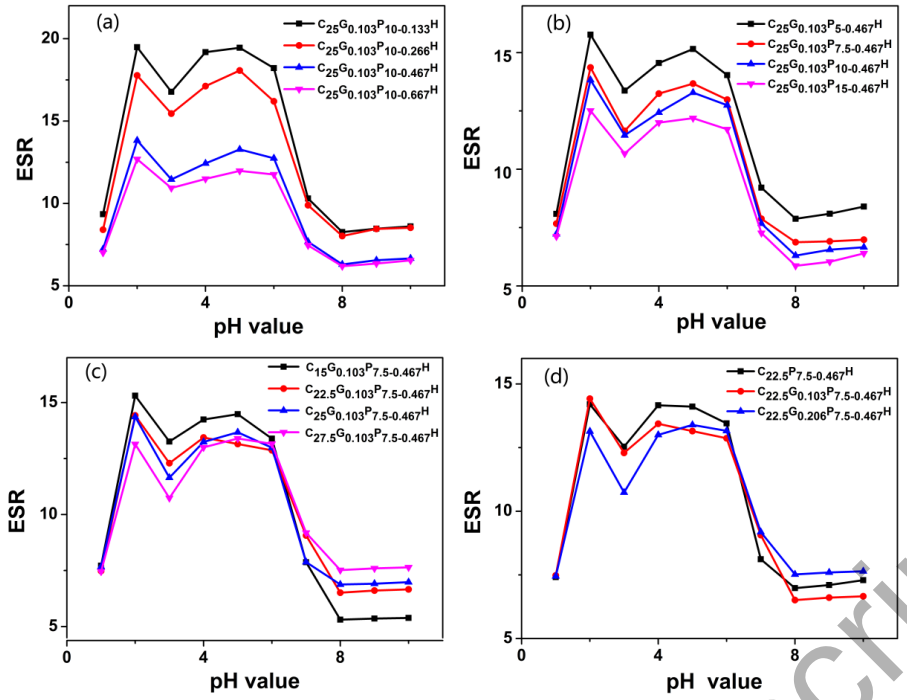

Fig. 7 ESR-pH value curves of synthesized hydrogel samples with different content of (a) BAC, (b) EDC, (c) CMCTs and (d) GO

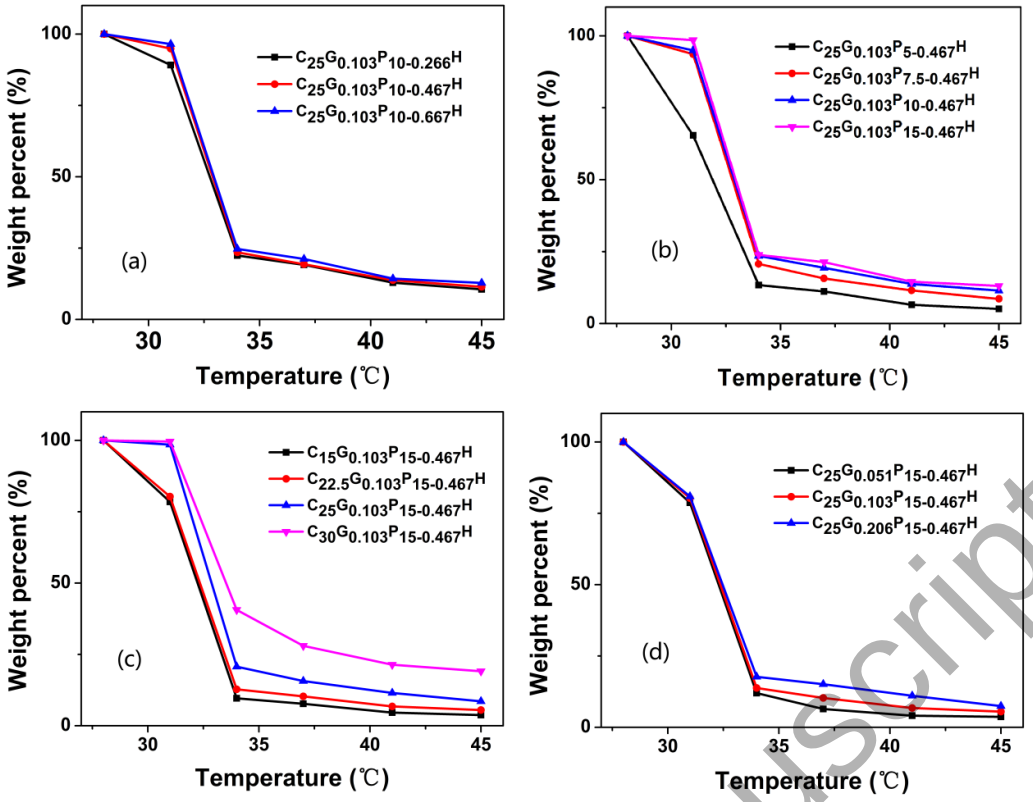

Fig. 8 The weight percent-temperature curves of synthesized hydrogel samples with different content of (a) BAC, (b) EDC, (c) CMCTs and GO content

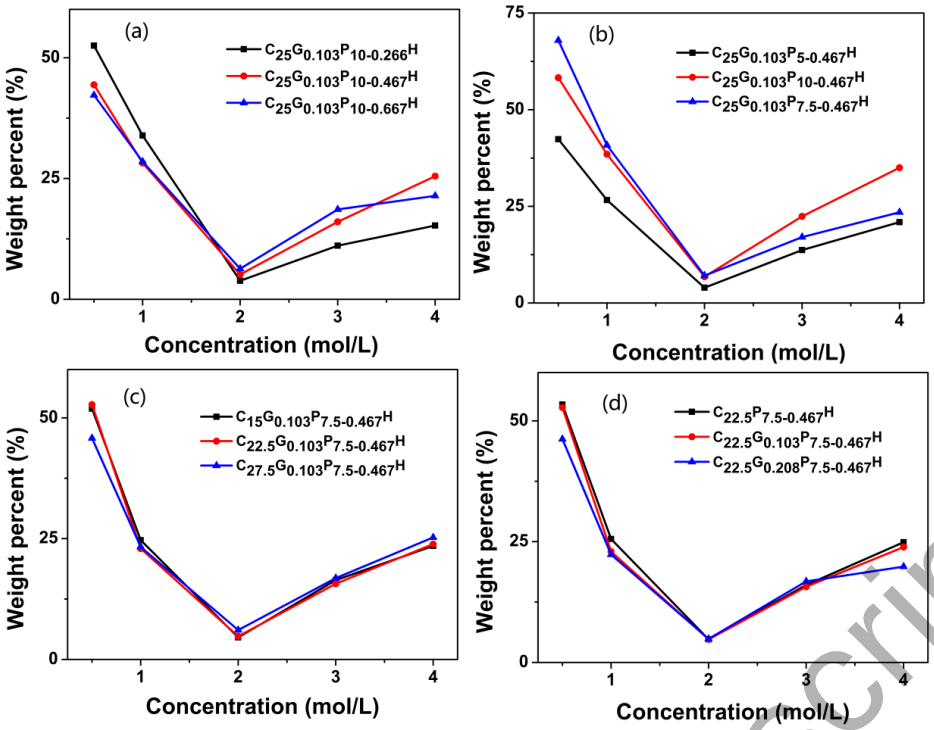

Fig. 9 The swelling behaviors of hydrogel samples with different content of BAC (a), EDC (b), CMCTs (c) and GO (d) in NaCl solutions with vary concentration

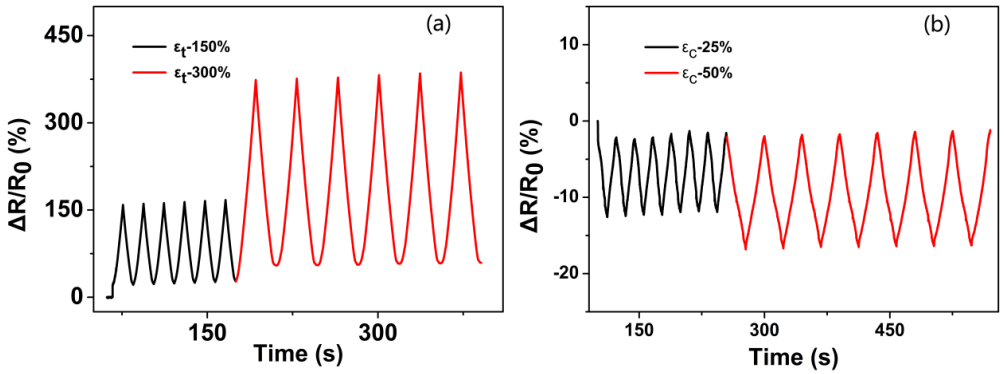

Fig. 10 The $\Delta R/R_0$-Time curves of optimal hydrogel samples under different tensile (a) and compressive (b) strains

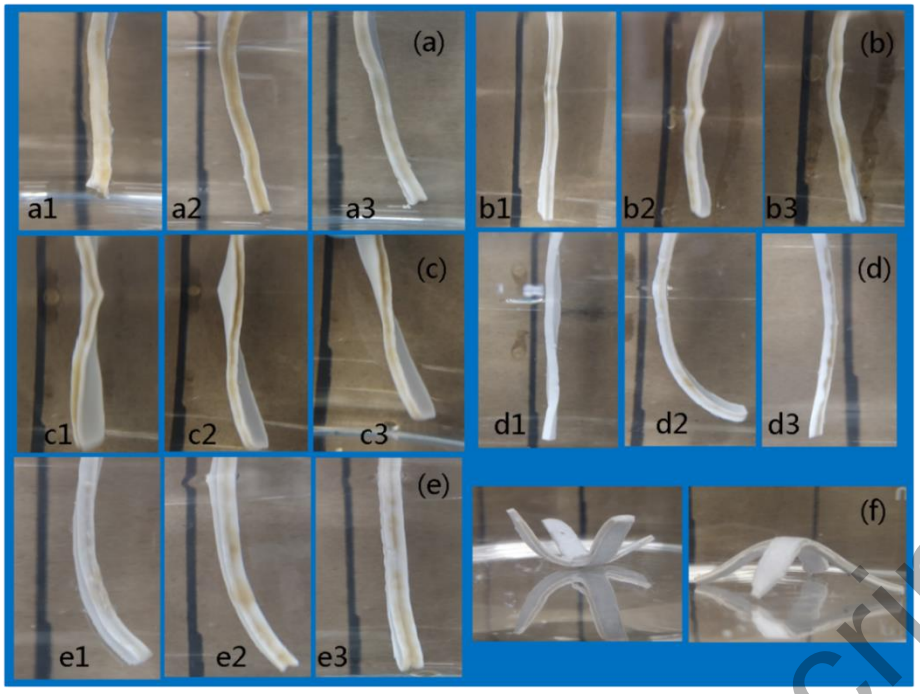

Fig.11 The images of synthesized bilayer hydrogel samples in 37℃(a-e) and 50℃(f) water bath, the detailed component are listed below: a1-$C_{25}G_{0.103}P_{10\text{-}0.133}/C_{25}G_{0.103}P_{10\text{-}0.133}$, a2-$C_{25}G_{0.103}P_{10\text{-}0.133}/C_{25}G_{0.103}P_{10\text{-}0.266}$, a3-$C_{25}G_{0.103}P_{10\text{-}0.133}/C_{25}G_{0.103}P_{10\text{-}0.467}$, b1-$C_{25}G_{0.103}P_{5\text{-}0.266}/C_{25}G_{0.103}P_{5\text{-}0.266}$, b2-$C_{25}G_{0.103}P_{5\text{-}0.266}/C_{25}G_{0.103}P_{10\text{-}0.266}$, b3- $C_{25}G_{0.103}P_{5\text{-}0.266}/C_{25}G_{0.103}P_{12.5\text{-}0.266}$, c1-$C_{15}G_{0.103}P_{6.5\text{-}0.266}/C_{15}G_{0.103}P_{6.5\text{-}0.266}$, c2-$C_{15}G_{0.103}P_{6.5\text{-}0.266}/C_{20}G_{0.103}P_{6.5\text{-}0.266}$, c3- $C_{15}G_{0.103}P_{6.5\text{-}0.266}/C_{25}G_{0.103}P_{6.5\text{-}0.266}$, d1-$C_{22.5}G_{0}P_{7.5\text{-}0.266}/C_{22.5}G_{0}P_{7.5\text{-}0.266}$, d2- $C_{22.5}G_{0}P_{7.5\text{-}0.266}/C_{22.5}G_{0.103}P_{7.5\text{-}0.266}$, d3-$C_{22.5}G_{0}P_{7.5\text{-}0.266}/C_{22.5}G_{0.206}P_{7.5\text{-}0.266}$, e-f $C_{20}G_{0.103}P_{7.5\text{-}0.266}/C_{25}G_{0.103}P_{15\text{-}0.467}$

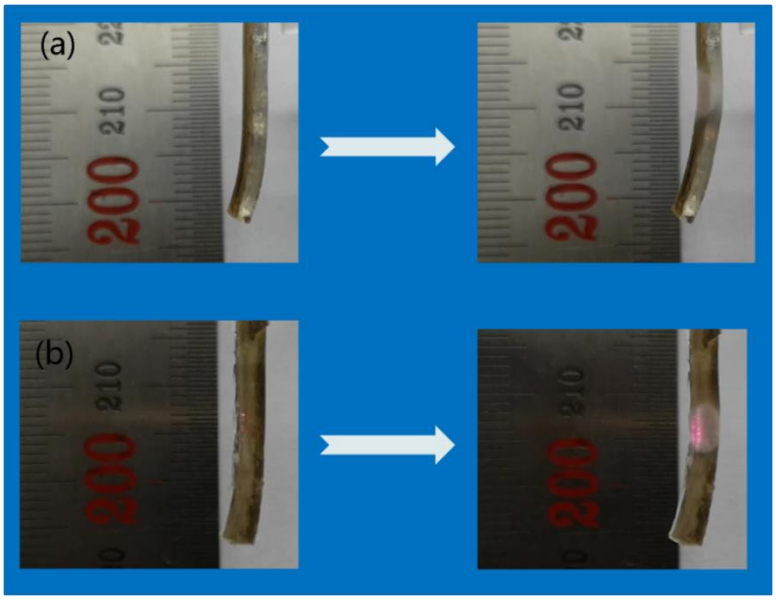

Fig.12 Bending images of the synthesized bilayer hydrogel samples with different component under 808 nm IR light. (a) $C_{22.5}G_0P_{7.5\text{-}0.266}/C_{22.5}G_{0.103}P_{7.5\text{-}0.266}$, (b) $C_{25}G_{0.103}P_{5\text{-}0.266}/ C_{25}G_{0.103}P_{12.5\text{-}0.266}$

Table1. Detailed component of the representative synthesized hydrogel samples

Samples	GO (μL)	MES (mL)	CMCTs (mg)	NIPAm(g)	BAC (mg)	EDC (mg)	NHS (mg)	I_{2959} (mg)
$C_{25}G_{0.051}P_{10\text{-}0.266}H$	50.00	4.95	125.00	0.59	1.35	50.00	12.50	5.60
$C_{25}G_{0.103}P_{10\text{-}0.266}H$	100.00	4.90	125.00	0.59	1.35	50.00	12.50	5.60
$C_{15}G_{0.103}P_{10\text{-}0.266}H$	100.00	4.90	75.00	0.59	1.35	50.00	12.50	5.60
$C_{25}G_{0.103}P_{7.5\text{-}0.467}H$	100.00	4.90	93.75	0.59	2.37	50.00	12.50	5.60

Table 2. Mechanical property of synthesized hydrogel samples

Hydrogel sample	Failure tensile stress (kPa)	Failure tensile strain (%)	Tenile modulus (kPa) (ε_t = 10-20%)	Compressive stress (MPa) (ε_c = 90 %)	Compressive modulus (kPa) (ε_c = 5 - 10%)
$C_{25}G_{0.103}P_{10\text{-}0.133}H$	150.12±1.51	727.37±2.07	3.19±0.09	0.99±0.08	1.11±0.09
$C_{25}G_{0.103}P_{10\text{-}0.266}H$	783.73±2.61	1381.74±5.62	4.55±0.12	1.62±0.10	5.65±0.12
$C_{25}G_{0.103}P_{10\text{-}0.4}H$	845.65±2.90	1366.71±6.15	6.34±0.15	--	--
$C_{25}G_{0.103}P_{10\text{-}0.467}H$	869.18±3.02	1228.36±4.12	7.45±0.18	4.98±0.13	7.44±0.15
$C_{25}G_{0.103}P_{10\text{-}0.533}H$	772.83±2.88	1018.74±3.31	7.72±0.21	--	--
$C_{25}G_{0.103}P_{10\text{-}0.667}H$	625.81±2.54	846.54±2.23	9.74±0.22	6.45±0.15	8.81±0.18
$C_{25}G_{0.103}P_{5\text{-}0.467}H$	441.55±2.36	830.14±2.96	5.97±0.19	2.13±0.09	4.76±0.12
$C_{25}G_{0.103}P_{7.5\text{-}0.467}H$	925.42±3.46	1262.67±5.31	6.3±0.20	3.04±0.13	6.73±0.16
$C_{25}G_{0.103}P_{15\text{-}0.467}H$	768.52±2.71	1049.78±3.43	7.58±0.24	8.35±0.21	8.55±0.20
$C_{25}G_{0.103}P_{20\text{-}0.467}H$	415.46±1.91	682.61±2.23	8.29±0.22	--	--
$C_{15}G_{0.103}P_{7.5\text{-}0.467}H$	601.77±2.32	1402.51±6.84	5.53±0.16	1.74±0.13	2.52±0.08
$C_{20}G_{0.103}P_{7.5\text{-}0.467}H$	784.88±2.83	1332.21±5.75	5.7±0.17	--	--
$C_{22.5}G_{0.103}P_{7.5\text{-}0.467}H$	1046.22±3.91	1286.76±6.42	6.58±0.24	2.37±0.20	6.10±0.17
$C_{27.5}G_{0.103}P_{7.5\text{-}0.467}H$	742.37±3.06	990.41±4.52	8.85±0.23	--	--
$C_{30}G_{0.103}P_{7.5\text{-}0.467}H$	532.25±2.62	573.61±2.54	11.51±0.31	4.21±0.16	10.04±0.25
$C_{22.5}G_{0.051}P_{7.5\text{-}0.467}H$	340.54±1.73	815.22±3.57	4.81±0.15	1.59±0.18	6.61±0.19
$C_{22.5}G_{0.155}P_{7.5\text{-}0.467}H$	845.17±3.86	1419.77±5.32	5.99±0.18	2.37±0.21	5.7±0.23